ELECTRICAL AND MICROSTRUCTURAL PROPERTIES OF ZnO-Bi_2O_3-TiO_2-Sb_2O_3-Al_2O_3-BASED VARISTOR CERAMICS FABRICATED BY SOLUTION COATING METHOD

R. MOHAMMADI[a,*], R. S.AZIS[a,b], A. ZAKARIA[a,b], N. H. ISA[a], N. K. SAAT[a], N. MOKHTAR[a], F.D. MUHAMMAD[a]

[a]*Department of Physics, Faculty of Science, Universiti Putra Malaysia, 43400 UPM Serdang, Selangor, Malaysia*

[b]*Materials Synthesis and Characterization Laboratory, Institute of Advanced Technology (ITMA), Universiti Putra Malaysia, 43400 UPM Serdang, Selangor, Malaysia*

This paper presents the electrical and microstructure properties of ZnO-Bi_2O_3-TiO_2-Sb_2O_3-Al_2O_3 varistor synthesized via solution coating technique. The mixed ZnO powder were sintered at 1250 °C in air at various holding time of 90, 120, 150, 180 and 240 min. The prepared powder was characterized by scanning electron microscopy (SEM), thermo gravimetric analysis (TGA), and particle size distribution. The results demonstrated that the ZnO composite powder is homogeneously coated and ultrafine. The densification, phase composition, and microstructure of ZnO varistors was studied by VPSEM, X-ray diffraction (XRD), and Energy-dispersive X-ray spectroscopy (EDX), respectively. The electrical parameters shows that 150 mins holding time has the highest value of nonlinear coefficient and (α = 16.93), highest value of breakdown electric field (E_b =66.35 V/mm) and the lowest values of leakage current (6.37×10^{-5} mA/cm^2). This result well documented that solution coating is a promising route to prepare ZnO varistors.

(Received August 7, 2018; Accepted December 3, 2019)

Keywords: ZnO, varistors, solution method, microstructure, electrical properties, holding time

1. Introduction

A polycrystalline zinc oxide (ZnO) based varistor ceramics are n-type semi-conductive ceramic. ZnO varistor ceramic commonly prepared by mixing and sintering ZnO powder with minor oxides additives such as V_2O_5, MnO_2, Nb_2O_5, MnO_2 , Gd_2O_3, Nd_2O_3[1,2], Bi_2O_3, TiO_2 [3, 4] , Co_2O_3, Sb_2O_3, Cr_2O_3, SiO_2 [5]; and rare earth Gd_2O_3, Nd_2O_3 [1,2]. ZnO varistor ceramics show excellent performance in terms of surge energy absorption capabilities, nonlinear coefficient parameter (α), nonlinear *J–E* (or *I–V*) response, and low leakage current characteristics. For this reason, ZnO varistor ceramics are widely used in electrical systems as surge protection devices to limit lightning and inner-overvoltage [10-11]. Homogeneous composites powder is important in ZnO varistor fabrication. Electrical properties of varistor are significantly influenced by the characteristics of preliminary powder. Homogeneous composite powders are hardly to obtain by conventional ball milling method. Several chemical methods have been introduced nowadays; such as chemical methods co-precipitation [7], sol–gel [8-10], microemulsion [11] and polymerized complex method [12].

Most of the chemical methods are complex and expensive, and they are inappropriate to produce the low-voltage ZnO varistors. Although, using of 'solution-coating' technique in preparation of high-voltage ZnO varistors has been reported [13-14]. Therefore, in this work an attempts to study the electrical property and microstructure of an addition of Bi^{2+}, Al^{2+}, Ti^{2+}, and Sb^{2+} ions in zinc oxide based varistor ceramics at various holding time by the solution coating

*Corresponding author: rabaah@upm.edu.my

methods will be investigate. In addition, the microstructure and electrical parameters such as current – voltage (*I–V*) curve of ZnO varistors were examined.

2. Experimental

2.1 Experimental procedure

The starting raw material used were zinc oxide (ZnO, 99.9%), bismuth nitrate ($Bi(NO_3)_3.5H_2O$, 98%), titanium butoxide ($Ti(OC_4H_9)_4$, 97%), antimony oxide (Sb_2O_3, 99.6%) and aluminium nitrate ($Al(NO_3)_3$, 98%), as listed in Table 1. The compositions of phases used in preparing varistors were the following:

ZnO phase: 98.6 mol% ZnO + 0.5 mol% of Bi^{2+}, 0.5 mol% of Ti^{2+} ions, 0.1 mol% of Al^{2+} ions and 0.3 mol% of Sb^{2+} ions.

Table 1. List of raw materials used in this study.

	ZnO	$Bi_2(NO_3)_3.5H_2O$	$(Ti(OC_4H_9)_4)$	$Al(NO_3)_3$	Sb_2O_3
Mol%	98.6	0.5	0.5	0.1	0.3
Purity%	99.9	99.999	97	98	99.6
Molecular Mass (g/mol)	81.39	485.11	340.32	375.13	291.5

The $Bi(NO_3)_3$ and $Ti(OC_4H_9)_4$ were mixed in a beaker and stirred in a 100 ml ethanol (C_2H_6O, 100%) for 1 h in room temperature. The ZnO powder was then added into the mixture and the temperature of the hot plate was increased to 85 °C. The solution was keep heat and stirred until it dry. The powder was again dried in an oven for 8 h at 150 °C. The dried powder was then agate mortar using mould and pestle to form a fined slurry powder. The powder were calcine for 2 h at 650 °C with heating and cooling rates of 5°C/mins. The calcined sample then crushed using agate mortar and adding the Sb_2O_3 powder. The powder were mould into a pellet shape of 10 mm diameter × 2 mm thickness with pressure of 2 ton/cm^2. The pellets were sintered at 1250 °C in air at 90, 120, 150, 180 and 240 min, with heating and cooling rates of 5 °C/min.

The thermal stability of the coating powders was obtained using TGA/DTG of Mettler Toledo Thermo Gravimetric Analyzer. The as-prepared powder was weighted about 10 mg and heated at operating temperature range from 30 °C - 1000 °C with heating rate 10 °C /min.

Phase formation of the powder and the sintered samples were characterized using X-ray diffraction (XRD) technique using a Philips X'pert PRO X-Ray Diffractometer Model PW3040 with Cu Kα radiation at 1.5418 Å. The range of diffraction angle used is from 20° - 80° at room temperature. The accelerating current and working voltage were 35 mA and 4.0 kV respectively. The data were analyzed by using an X'Pert High Score Plus software. The average density (ρ) of sintered sample was determined using an electronic densimeter (Alfa Mirage, Model MD-300S), working based on the Archimede's principle.

The microstructures of the powder and the sintered samples were examined by variable pressure scanning electron microscope (VPSEM) in which the specimens were coated with gold for observation. The elements present in the various phases were identified using EDX spot analysis.

The current density (*J*)-electric field (*E*) characteristics were measured at room temperature using a low-voltage source-measure unit (Keithley Model 2410) to obtain a non-linear coefficient (α). The measurement was performed by varying the applied voltage from 0 to 100 V. All samples were coated with silver conductive paint and cured at 550 °C for 10 mins to make the electrodes. The nonlinear α value was determined from *J-E* plot through the expression Eq. (1):

$$\alpha = \frac{\log J_2 - \log J_1}{\log E_2 - \log E_1} \quad (1)$$

where J_1 and J_2 are current densities and E_1 and E_2 are electric fields in line with J_1 and J_2 at 0.1, and 1 mA/cm^2, respectively. All the sample was measured with dc voltage from 0 to 100 V in step size of 2.5 V. Current (I) and voltage (V) can also be used in place of current density (J) and electric field (E), but the resultant values for nonlinear coefficient α are the same if both parameters are used [15]. The leakage current (J_L) was measured at $0.85V_1$ mA. The breakdown voltage, E_b was determined by measuring E at J = 1 mA/cm^2. From the J-E curve the varistor electric field ($E_{1mA)}$ was determined at a current of 1 mA, the leakage current density (J_L) is obtained at $0.85E_{1mA}$.

3. Results and discussion

The thermogravimetric analyses (TGA) of ZnO composite ceramics prepared via solution coating synthesis is shown in Fig. 1. The TGA curve show three (3) decomposition processes; at 100 °C, 195 °C, 300 °C, and 500 °C which represent exothermic peaks. The weight loss at temperature 100 °C corresponds to the decomposition process due to dehydration of the absorbed water. The second exothermic peaks at 300 °C is attributed to the decomposition of the residual organic compounds which tends to liberate H_2O, O_2, and NO component. The exothermic peaks at 500 °C is attributed to the decomposition of hydroxides and organic matter which is the formation of several metal oxide. The endothermic peak of the TGA peaks shows the formation of ZnO nanopowder occurred at 500 °C. The similar results also agreed with previous reported by Li et.al [16]. The TGA curve illustrates the weight sharply reduces with the temperature up to 450 ^oC and the weight remains constant above that temperature. There is a sharp exothermic peak at 500 °C on the DTG curve, be consistent with an exothermic reaction (for the combustion of nitrates, acetates and citrate). The spectrum indicates a good temperature for calcination to be above 600 °C, therefore, a calcinations treatment at 650 °C was employed for the as-prepared powders.

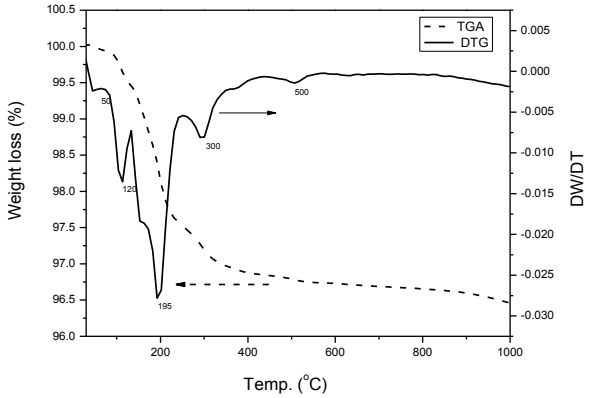

Fig. 1. TGA/DTG analysis of ZnO composite powders.

Fig. 2 shows the XRD patterns of the ZnO mixed powder for powder after calcination from the solution coating route. The 2θ reflection pattern at 31.7494°, 34.4129°, 36.2412°, 47.5531°, 56.6025°, 62.8749°, 66.3733°, 67.9546°, 69.0849° and 76.9675° are represent the polycrystalline ZnO varistor and label as '*'. The patterns confirmed the presence of dominant ZnO phase (ICSD code: 98-006-5190) with hexagonal structure and a space group of P 63 m c. There are many secondary phases with small peaks were detected in the polycrystalline ceramic at all holding time, marked as 'Δ'. These peak are matched to the reflection of $Bi_4Ti_3O_{12}$ (ICSD code:

98-005-3095), $ZnAl_2O_4$ (ICSD code: 98-006-6231), Zn_2TiO_4 (ICSD code: 98-003-8423) and Sb_2O_4 (ICSD code: 98-010-3908). These results are similar to previously reported by Li et.al [16] and Dorraj et. al [17].

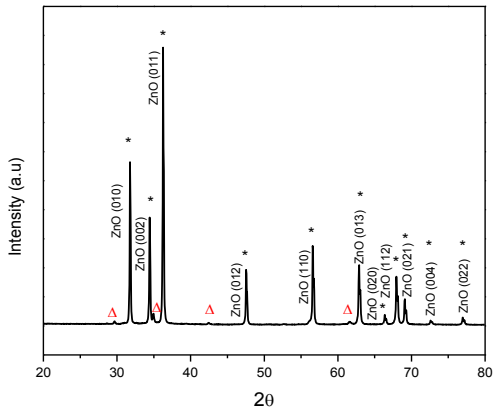

Fig. 2. XRD patterns of mixed powder after calcined at 650 ^oC.

Fig. 3 shows the SEM morphology images of ZnO powder for before and after solution coating synthesis. The particle size were observed in range of 100 to 400 nm with the mean grain size of about 300 nm. It is observed the presence of compound are coated on the ZnO surface. It is evident that the presence of the additives in ZnO grains, and the additives particle size are much smaller compared to the size of ZnO particles. The similar results from previously reported by Yi. et al. [16]. The SEM morphology after solution coating shows the larger grains represent ZnO grains and the size of ZnO grains nearly unchanged. After solution coating process, the ZnO grains surface is rough and coated by the additives. The size of the additives show small compared to ZnO particles.

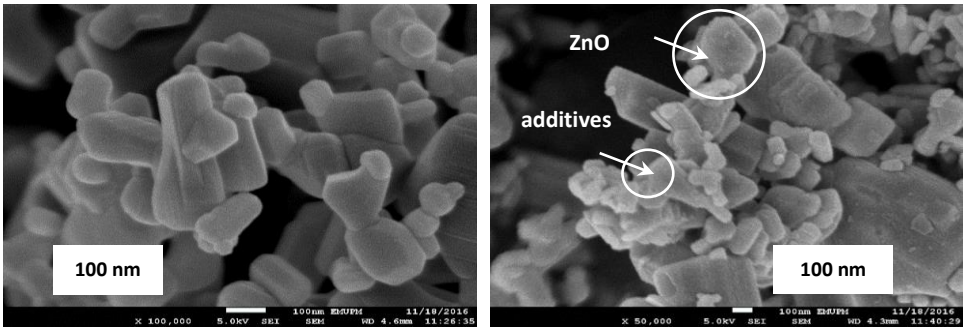

a) *b)*

Fig. 3. The FESEM images of ZnO powder (a) before and (b) after solution coating process.

Fig. 4 shows the SEM images of sintered ZnO mixed ceramics at various holding time. The grain size of the sample was found to increase from 3 to 15 μm, as increase the holding time. It can be explained that the enlargements of grain size at high holding time decrease the grain boundaries. This results also affect the varistor nonlinearity (Fig. 8, Table 1). As increase the holding time, the grain start to grow and increase the grain size. The increase of grain size introduce less grain boundaries. It should be noted that the grain size was measured by randomly oriented boundaries. Particle size and size distribution of powders are important in varistor characterization. This because they have significant effects on the density, electrical and thermal properties of the varistors. If the particle size distribution of the ZnO varistor is wide, therefore, the growing rate of ZnO grains is different and leading to the rearrangement of the ZnO grains. This mechanism will lead to the formation of pores in the sintered varistors. Many grain

boundaries are liable to modified electrical properties and improve diffusion, while less grain boundaries are free to isolation atoms and are electrically in active [19]. At the lower holding time (120 min), the grain size was not clearly pronounced but it was more clear once the holding time increased by 150 min. However, grain size increased as the sintering holding time reached 180 min. According to the EDX results (Fig. 5), the other dopants such as TiO_2 and Al_2O_3 are mostly located in the grain boundaries consistent with the previous studies [12,13]. The best marks are related to EDX micrograph and spectrum of the validated varistor at 150 min. The Ti , Sb, and Al are found at grains boundaries while Bi hidden. Previously reported that the Bi_2O_3 acts as grain enhancer and produces the boundary state and nonlinearity effects [20]. While TiO_2 is commonly used as the grain-growth-enhancing additive in low-voltage varistor ceramics [21]. Density of polycrystalline mixed ZnO varistors at various holding time were observed 5.34 to 5.62 g/cm^3. Fig. 6 shows the density of the mixed ZnO varistors as increase the holding time. The density decreasing is relevant to the vaporization of Bi_2O_3 at high temperature [7, 23, 24], while the growth of ZnO grains at high temperature leads to the decrease of breakdown field. Holding time of 150 mins shows the maximum density value of 5.62 g/cm^3.

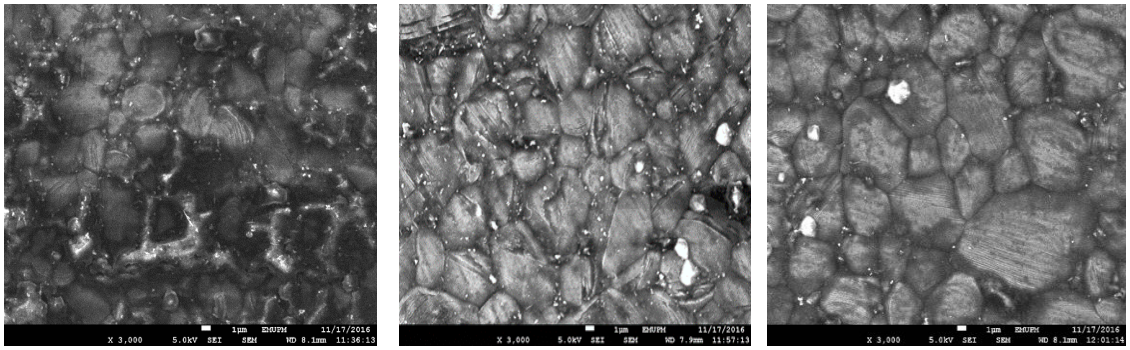

a) *b)* *c)*

Fig. 4. SEM micrograph for solution coating method of sintered ZnO varistor in different holding time: a) 120 min, b) 150 min, c) 180 min

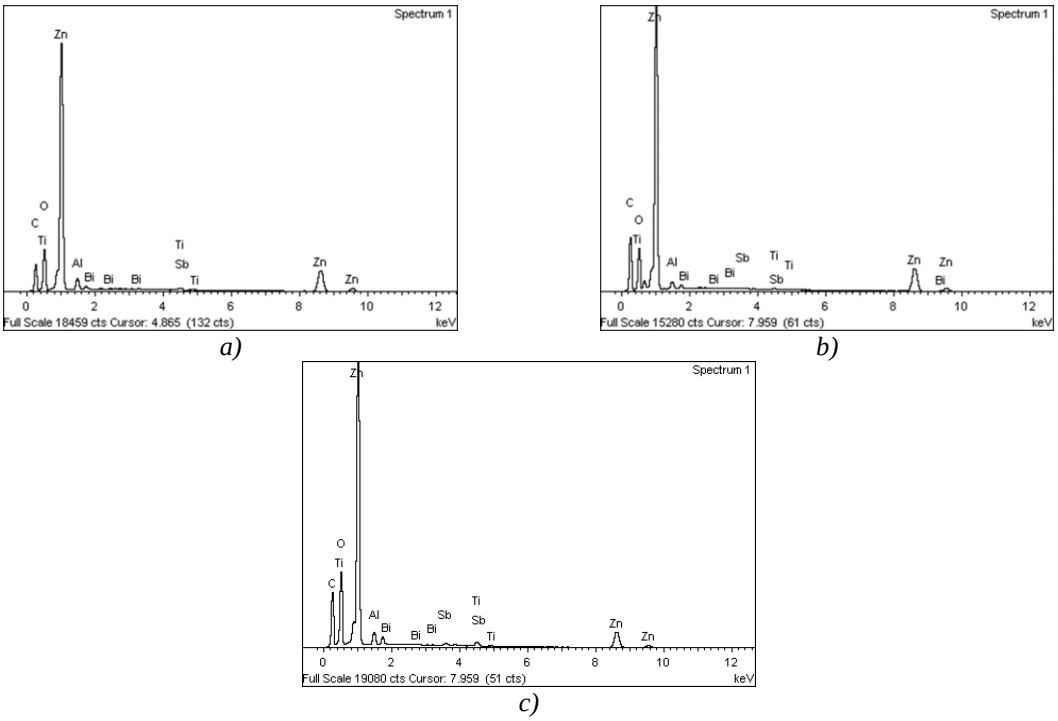

a) *b)*

c)

Fig. 5. EDX for solution coating method of ZnO varistor in different holding

Time: a) 120 min, b) 150 min, c) 180 min

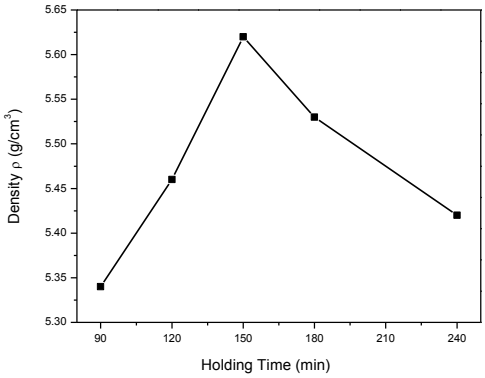

Fig. 6. Density for solution couting method ZnO varistor at different holding time (90, 120,150 and 180 min).

Table 1. Average grain size D, percentage density ρ, and nonlinear coefficient α and breakdown electric field E_b and leakage current J_L for solution coating varistor ceramic at various holding time.

Sintering Holding Time (min)	*D* (μm)	ρ (%)	α	E_b *(V/mm)*	J_L *mA/cm²*
90	-	5.34	14.3	28.3	9.77×10^{-5}
120	23.55	5.46	15.75	37.4	7.78×10^{-5}
150	29.13	5.62	16.93	66.35	6.37×10^{-5}
180	36.7	5.53	14.63	26.45	9.23×10^{-5}
240	-	5.42	11.88	16.47	1.40×10^{-4}

Fig. 6 depicts the distribution and shape of *J-E* characteristic curves for the ZnO ceramics. ZnO varistor ceramics has the non-ohmic electrical properties. The non-ohmic property's degree is define by a nonlinear coefficient α. The α value can be determine from the slope of the graph of log current density (log *J*) versus log field strength (log *E*) (Equation 2),

$$\alpha = \frac{\log J}{log\ E} \qquad (2)$$

Fig. 7 shows the current density *J* versus electric field *E* graph of ZnO- ZnO-Bi_2O_3-TiO_2-Sb_2O_3-Al_2O_3-based varistor ceramics synthesized by solution coating method sintered at different holding time. The curves is shifted to the higher electrical field region as increase the holding time. The 180 min holding time shows the more shifted to higher electric field. The ZnO-based varistor ceramics holding time 150 min exhibited most pronounced nonlinear properties in the vicinity of the knee. The sharp knee of the curves indicating good varistor properties. The *J-E* parameters which obtained from the characteristic curves are summarized in Table 2.

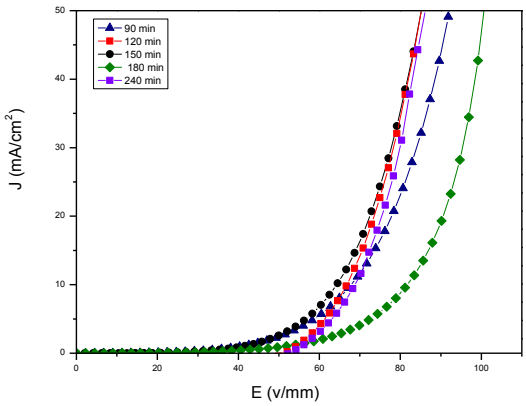

Fig. 7. J-E characteristics of ZnO solution coating varistor sintered at different holding time (90, 120,150 and 180 min).

Fig. 8 and Fig. 9 shows the nonlinear coefficient α and breakdown field E_b of ZnO varistor at various holding time, respectively. The nonlinear coefficient is very important parameter for characterizing the nonlinearity of the varistor ceramic. The α and the breakdown electric field (E_b) were identified from the *J-E* characteristic curves. As the holding time is increased, the nonlinear coefficient markedly increased (Table 2). The maximum value of the nonlinear coefficient was found for 150 min holding time. There was a decline trend in the breakdown field from 28.30 to 16.47 V/mm when holding time was elevated up to 240 min and the α reached to its lowest value (Fig. 8). Obviously, the holding time has influence on electrical properties of varistors. There were significant differences in electrical parameters of the investigated samples of nonlinear coefficient α ranging from 14.3 to 16.93, and breakdown field E_b from 16.47 to 66.35 V/mm. The graph suggest that 150 min holding time has the best electric properties, with the highest value of nonlinearity coefficients (α = 16.93), highest value of breakdown electric field (E_b =66.35 V/mm) and the lowest values of leakage current (6.37×10^{-5} mA/cm^2). On the other hand, sample 240 min holding time showed poor electrical properties, with the lowest nonlinear coefficient (α = 11.88) and high leakage current. The homogenous microstructures and the micron size of the crystalline grains are greatly the factors contribute to the large nonlinearity coefficients of varistors.

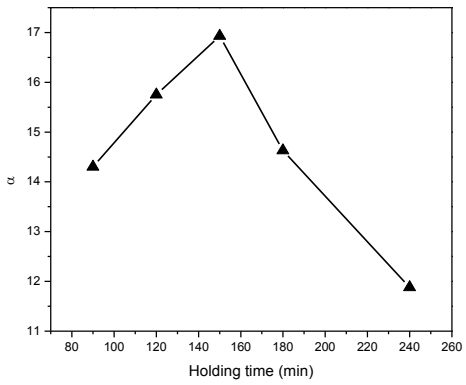

Fig 8. Nonlinear coefficient α against holding time of ZnO solution coating varistor

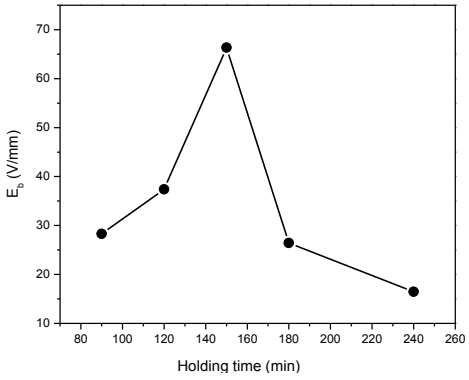

Fig. 9. Breakdown voltage E_b against holding time of ZnO solution coating varistor.

4. Conclusions

In conclusion, ZnO-Bi_2O_3-TiO_2-Sb_2O_3-Al_2O_3-based varistor ceramics fabricated by a solution coating method has presented. The effect of holding time from 90 to 240 min on the microstructure and electrical properties of this varistor ceramics has been investigated. This technique is a novel method to produce the composite powder for high performance ceramics. The properties of preliminary ZnO composite powder was studied by SEM, TGA, and particle size analysis. The threshold voltage of the varistors prepared through solution coating was 66.37(V/mm) that was much higher than that of conventional prepared varistors. The optimum nonlinear coefficient α of the varistors obtained is 16.93. For solution technique, the optimum values of Bi_2O_3, TiO_2, Sb_2O_3 and Al_2O_3 in maximum alpha are at the holding time of 150 min.

Acknowledgements

The authors are grateful to the Universiti Putra Malaysia for supporting this work under the Putra Grants (UPM/700-1/2/GPPI/2017/954160, GP-IPS 9580600/9533300, GP/2018/ 9628400) and Fundamental Research Grants Scheme (FRGS/2016/5524942), Ministry of Education, Malaysia for the financial support.

References

[1] N. H. Isa, A. Zakaria, R. S. Azis, W. R. W. Abdullah, Digest Journal of Nanomaterials and Biostructures **12**(3), 821 (2017).
[2] N. H. Isa, A. Zakaria, R. S. Azis, Z. Rizwan, Solid State Phenomena **268**, 181 (2017).
[3] G. M. Sabri, B. Z. Azmi, Z. Rizwan, M. K. Halimah, M. Hashim, M. H. M. Zaid, International Journal of Physical Sciences **6**(6), 1388 (2011).
[4] Y. Abdollahi, A. Zakaria, R. S. Azis, S. N. A. Tamili, K. A. Matori, N. M. M. Shahrani, N. M. Sidek, M. D. S. Moosavi, Chemistry Central Journal **7**, 137 (2013).
[5] T. K. Gupta, Ferroelectrics **102**(1), 391(1990).
[6] Z. Dongxiang, C. Zhang, S. Gong, Materials Science and Engineering: B **99**(1-3), 412 (2003).
[7] H. Özkan Toplan, Y. Karakaş, Ceramic International **27**(7), 761 (2001).
[8] J. Zhang, S. Cao, R. Zhang, L. Yu, C. Jing, Current Applied Physics **5**(4), 381 (2005).
[9] Ya, K. Xue, W. T. Diao, Y. Han, T. M. De, T. M. Jing, Material Research Bulletin **32**(9), 1165 (1997).
[10] S. Y. Chu, T. M. Yan, S. L. Chen, Ceramic International **26**(7), 733 (2000).
[11] M. Singhai, V. Chhabra, P. Kang, D. O. Shah, Material Research Bulletin **32** (2), 239 (1997).
[12] Duran, Pedro, F. Capel, J. Tartaj, C. Moure, Advanced Materials **14** (2), 137 (2002).

[13] Banerjee, Arundhati, T. R. Ramamohan, M. J. Patni, Material Research Bulletin **36**(7-8), 1259 01).
[14] Li, Yuke, G. Li, Q. Yin, Material Science and Engineering B 130 (1-3), 264 (2006).
[15] B. Ai, H. T. Nguyen, A. Loubiere, Journal of Physics D Applied Physics **28** (4), 774 (1995).
[16] Y. Li, G. Li, Q. Yin, Materials Science and Engineering B **130**, 264 (2006).
[17] M. Dorraj, A. Zakaria, Y. Abdollahi, M. Hashim, S. Moosavi, The Scientific World Journal, 741034 (2014).
[18] M. Wang, Y. Chao, Z. Nan-fa, Journal of Materials Processing Technology **202**(1-3), 1039 (2008).
[19] Eda Kazuo, Journal of Applied Physics **56**(10), 2948 (1984).
[20] Olsson Eva, Gordon L. Dunlop, Journal of Applied Physics **66**(9), 4317 (1989).
[21] Daneu Nina, A. Rečnik, S. Bernik, Journal of American Ceramic Society **86**(8), 1379 (2003).
[22] Bui Ai, H. T. Nguyen, A. Loubiere, Journal of Physics D: Applied Physics **28** (4), 774 (1995).
[23] Suzuki, Hironori, R. C. Bradt, Journal of American Ceramic Society **78**(5), 1354 (1995).
[24] Wong Joe, Journal of Applied Physics **51**(8), 4453 (1980).